The Journal of Chemical Physics

# Photoexcited organic molecules *en route* to highly efficient autoionization

Cite as: J. Chem. Phys. **152**, 074715 (2020); https://doi.org/10.1063/1.5136075
Submitted: 11 November 2019 . Accepted: 24 January 2020 . Published Online: 20 February 2020

Sesha Vempati, Lea Bogner, Clemens Richter, Jan-Christoph Deinert, Laura Foglia, Lukas Gierster, and Julia Stähler

The Journal of Chemical Physics ARTICLE scitation.org/journal/jcp

# Photoexcited organic molecules *en route* to highly efficient autoionization

Cite as: J. Chem. Phys. 152, 074715 (2020); doi: 10.1063/1.5136075
Submitted: 11 November 2019 • Accepted: 24 January 2020 •
Published Online: 20 February 2020



Sesha Vempati,[a] Lea Bogner, Clemens Richter, Jan-Christoph Deinert,[b] Laura Foglia,[c] Lukas Gierster, and Julia Stähler[d]

## AFFILIATIONS

Fritz Haber Institute of the Max Planck Society, Faradayweg 4-6, 14195 Berlin, Germany

**Note:** This paper is part of the JCP Special Topic on Ultrafast Molecular Sciences by Femtosecond Photons and Electrons.
[a]**Present address:** Indian Institute of Technology Bhilai, Chhattisgarh, India.
[b]**Present address:** Helmholtz-Zentrum Dresden-Rossendorf, Dresden, Germany.
[c]**Present address:** Elettra-Sincrotrone Trieste S.C.p.A, Basovizza, Italy.
[d]**Author to whom correspondence should be addressed:** staehler@fhi-berlin.mpg.de

## ABSTRACT

The conversion of optical and electrical energies in novel materials is key to modern optoelectronic and light-harvesting applications. Here, we investigate the equilibration dynamics of photoexcited 2,7-bis(biphenyl-4-yl)-2′,7′-ditertbutyl-9,9′-spirobifluorene (SP6) molecules adsorbed on ZnO(10-10) using femtosecond time-resolved two-photon photoelectron and optical spectroscopies. We find that, after initial ultrafast relaxation on femtosecond and picosecond time scales, an optically dark state is populated, likely the SP6 triplet (T) state, that undergoes Dexter-type energy transfer ($r_{Dex}$ = 1.3 nm) and exhibits a long decay time of 0.1 s. Because of this long lifetime, a photostationary state with average T–T distances below 2 nm is established at excitation densities in the $10^{20}$ cm$^{-2}$ s$^{-1}$ range. This large density enables decay by T–T annihilation (TTA) mediating autoionization despite an extremely low TTA rate of $k_{TTA} = 4.5 \cdot 10^{-26}$ m$^3$ s$^{-1}$. The large external quantum efficiency of the autoionization process (up to 15%) and photocurrent densities in the mA cm$^{-2}$ range offer great potential for light-harvesting applications.



## I. INTRODUCTION

Electronic and excitonic couplings between the excited states of molecules and across hybrid interfaces[1] are vital aspects for various applications such as photovoltaics,[2,3] photochemical reactions,[4] solar energy conversion,[5] and opto-electronics.[6] The strength and nature of coupling between any two excited states as well as the energy level alignment at an interface are dependent on the molecular architecture, the degree of molecular order, and bonds, as well as molecular arrangements at interfaces.[7–10] One overarching goal of all these applications is the conversion of energy while minimizing energy losses. Particularly when aiming at the exploitation of solar radiation, this is a major challenge as the bandgap of the absorbing species sets a lower boundary for the convertible photon energies while high energy photons are absorbed, but a significant portion of their energy is dissipated as heat.[11] One approach to maximize the number of charge carriers generated by light is to use singlet fission, where a high energy singlet state decays into two triplet states, thereby duplicating the number of charge carriers that can be harvested.[12] In the inverse process, triplet–triplet annihilation (TTA) through photon upconversion, two triplets interact by an electron-exchange Dexter mechanism that populates a singlet exciton at higher energy. Recombination leads to emission of an upconverted photon,[2–5,8,13–16] which can, for instance, drive photochemical reactions or, in the case of incident infrared radiation, to the generation of visible photons that can be harvested by conventional solar cells.[15]

Whether or not TTA occurs in organic compounds depends on many aspects. For instance, anthracene solutions exhibit photon upconversion,[8] whereas the crystalline counterpart shows autoionization.[9,10] The latter can be induced by various excited state coupling schemes: Singlet/singlet exciton (singlet fusion),[17,18] free electron/charge-transfer exciton (CTX),[16] CTX–CTX annihilation,[9] or free electron/singlet exciton,[10] as observed in naphthalene

trimer,[17] perylene films,[7] and fluoranthene crystals.[18] In these cases, the higher excited singlet is above the vacuum level, while, notably, the excitation energies are lower than the first ionization potential of the molecules. Remarkably, to our knowledge, autoionization[19] mediated by TTA has not been observed to date.

For both photon upconversion and autoionization, the cooperative interaction of two excited states provides the required energy, while their lifetimes, densities, and mobilities determine if the promotion of the electron to the higher excited state is possible. Energy transfer in organic compounds usually occurs by either a Förster or a Dexter mechanism, while the former process mostly occurs in the case of singlet and the latter in the case of triplet excitations. The Förster transfer, which occurs via dipole–dipole interaction, shows a rate constant,[20]

$$k_F(r) = k_D\left(\frac{r_F}{d}\right)^6, \tag{1}$$

which is determined by the distance between the donor and the acceptor $d$, the excited state lifetime $\tau_D = (k_D^{-1})$, and the Förster radius $r_F$, at which 50% of the excitations transfer to the accepting molecule. In the case of Dexter transfer, the energy is transferred by two charge-transfer processes. For Dexter-type TTA, energy is transferred from one excited (triplet) state to another excited (triplet) state, which leads to one molecule in the ground state and the other one in a doubly excited state. The latter subsequently decays in an Auger-like process by promoting one electron to the ground state level and the other one to a higher excited state. The two initial charge transfer processes require wave function overlap, which is why Dexter transfer is a short-range process, usually occurring across few nanometer distances. The rate constant can be written as[20]

$$k_{Dex}(r) = k_D \cdot \exp\left(\frac{2r_{Dex}}{L}\left(1 - \frac{d}{r_{Dex}}\right)\right), \tag{2}$$

where $L$ is the van der Waals distance of the molecules and $r_{Dex}$, analogous to Förster transfer, the distance at which 50% of the excitations transfer to the accepting molecule. This results from the quantum yield for energy transfer,

$$\Phi_{ET}(r) = \frac{k_{ET}(r)}{k_{ET}(r) + k_D}. \tag{3}$$

Another type of energy transfer that can lead to electron emission is Auger decay. It is a one-step process where one excited electron absorbs the energy of another one nearby. This process is, even more than Dexter transfer, a short-range phenomenon, in which the contributing carriers need to be localized on neighboring atoms and which can be excluded for distances larger than 2 Å.[21,22]

Equations (1) and (2) illustrate the importance of the lifetime $\tau_D$ of the excited state. It can be reduced when the molecules are adsorbed on an inorganic substrate as interfacial charge separation competes with the intrinsic dynamics of the excited molecules.[6,23,24] One example is our earlier work on 2,7-bis(biphenyl-4-yl)-2′,7′-ditertbutyl-9,9′-spirobifluorene (SP6) molecules grown on a ZnO(10-10) substrate.[24] SP6 grows with $\rho = 1.14 \cdot 10^{27}$ m$^{-3}$ in quite dense amorphous films,[25] and its absorption sets in at 3.2 eV and is maximal at 3.6 eV.[23] Femtosecond time-resolved optical

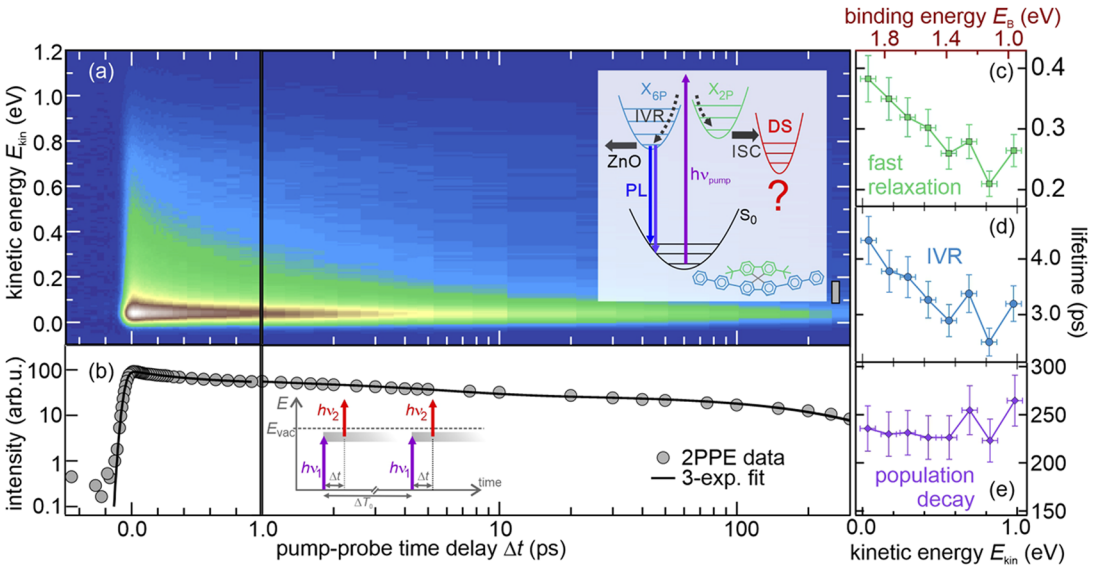


**FIG. 1**. (a) Photoinduced photoelectron intensity (false colors) after subtraction of the constant single color background of 21 nm SP6/ZnO(10-10). The data are plotted as a function of pump–probe pulse time delay (horizontal axis) and kinetic energy (vertical axis) measured using $h\nu_{pump}$ = 3.86 eV and $h\nu_{probe}$ = 1.93 eV. Inset: elementary processes following optical excitation of SP6 molecules: internal vibrational relaxation (IVR), photoluminescence (PL) through electron–hole recombination of excitons in the 6P unit of the molecules ($X_{6P}$) competing with charge separation at the SP6/ZnO interface, and intersystem crossing (ISC) to the dark state. (b) Exemplary, energy-integrated ($E_{kin}$ = 0.11–0.23 eV) cross correlation trace (electron intensity as a function of time delay, gray markers) and a triple-exponential fit (black). The inset shows the pump–probe scheme at a pump–probe time delay $\Delta t$ and inverse repetition rate $\Delta T$. Panels (c)–(e) depict the energy dependent fit parameters.

spectroscopy combined with photoluminescence (PL) spectroscopy unveiled that weak electronic coupling between singlets localized on the sexiphenyl (6P) and the spiro-linked biphenyl (2P) moiety of SP6 leads to two independent relaxation pathways as illustrated by the inset in Fig. 1(a).[24] The recombination of the exciton localized on the sexiphenyl unit ($X_{6P}$, blue) leads to photoluminescence (PL), which is limited by charge separation at the ZnO interface. This PL exhibits a vibrational progression that likely results from a coupling to the CC-stretch and CH-bend modes of the central fluorenes of SP6.[26] In addition, photoexcitation also leads to the population of the biphenyl unit ($X_{2P}$, green) that does not decay by light emission, but serves as an intermediate state in the formation process (230 ps) of a dark state (DS) with a lifetime exceeding 5 $\mu$s. Unfortunately, neither the origin, energetic position, nor the coupling of this DS to other states could be accessed in these previous experiments.[24]

It is worth noting that understanding of photostationary states with lifetimes exceeding the inverse repetition rate of the laser system as described above can also be highly relevant with regard to a correct interpretation of the *ultrafast* dynamics in a system, as the latter may represent the relaxation of the sample to an excited (photostationary) state, not the ground state.

In the present study, we unfold the dynamics in SP6 molecules following optical excitation using tr-2PPE spectroscopy. Remarkably, the evolution of the femtosecond time-resolved photoelectron intensity coincides with the previously observed ultrafast dynamics in the optical experiments. Moreover, we show that the 2PPE spectra are dominated by a spectral signature that originates from the autoionization of the SP6 molecules, which is a consequence of the cooperative interaction of two SP6 molecules in the DS, which is likely the triplet state. A simple rate equation model reproduces the non-linear excitation density dependence of the electron emission intensity and supports autoionization of SP6 molecules through TTA. We show that the DS decays with a large time constant of 0.1 s and determines the rate constant for TTA to be $k_{TTA} = 4.5 \cdot 10^{-26}$ m$^3$ s$^{-1}$. The TTA is mediated by Dexter energy transfer with $r_{Dex} = 1.3$ nm that is enabled by the long lifetime of the excitation and the large density of the SP6 molecules. The resulting electron emission has a large external quantum efficiency (EQE) of up to 15% and a photocurrent density of 1.5 mA/cm$^2$ at solar UV photon fluxes. Considering that these competitive values result from a mono-molecular organic film, electron emission through TTA might be a promising route for future light-harvesting devices.

## II. EXPERIMENTAL DETAILS

The samples are prepared in an ultrahigh vacuum (UHV) chamber operating at a base pressure of $10^{-10}$ mbar. The ZnO(10-10) surface (MaTecK GmbH) is cleaned by repeated cycles of Ar + sputtering (10 min, $p_{Ar} = 2.0 \cdot 10^{-6}$ mbar, 750 eV at 300 K) followed by 30 min annealing at 950 K (ramping rate of 30 K/min). The SP6 molecules purchased from Merck are thoroughly outgassed and evaporated at 580 K from a Knudsen cell onto a freshly prepared surface (at 300 K) to form amorphous films with nominal thicknesses of up to 25 nm. A precalibrated quartz crystal microbalance is employed to determine the thickness of the film. For 2PPE spectroscopy, these samples are transferred *in situ* into the neighboring analysis chamber (base pressure $10^{-11}$ mbar); for optical spectroscopy, they are moved through air to an optical cryostat with a base pressure of $10^{-6}$ mbar. In all the reported measurements, the sample was kept at 100 K using liquid nitrogen.

Static and time-resolved 2PPE experiments are performed using a regeneratively amplified femtosecond (40 fs pulses) laser system (Ti:Sa, Coherent RegA, 40–200 kHz) which provides a fundamental photon energy of 1.55 eV. The repetition rate ($1/\Delta T_0$) of the laser determines the time-duration $\Delta T_0$ between two subsequent pulses h$\nu_1$; see the inset of Fig. 1(b). A fraction of the total power is directed to an optical parametric amplifier which generates photon energies from 1.85 eV to 2.55 eV. 3.10 eV, 4.65 eV, and 6.2 eV photons are obtained by frequency doubling, tripling, and quadrupling the 1.55 eV energy photons, respectively, while 3.45 eV, 3.62 eV, 3.85 eV, and 4.11 eV photons are obtained by frequency doubling of the output of the optical parametric amplifier. The pulse duration is evaluated from the high energy photoemission cross correlation signal of two laser pulses on a clean tantalum foil inside the UHV chamber. The kinetic energy ($E_{kin}$) and intensity of the emitted electrons are detected using a hemispherical electron analyzer (PHOIBOS 100, SPECS GmbH) and referenced to the Fermi energy ($E_F$) of the tantalum sample holder which is in electrical contact with the sample surface. A bias voltage of −1.0 V with respect to the analyzer is applied to the sample enabling the detection of electrons of zero $E_{kin}$. As discussed in detail previously,[27] the low energy secondary electron cutoff ($E_S$) in the photoelectron spectra provides the work function ($\Phi$) of the surface when the spectra are plotted as a function of final state energy axis with respect to $E_F$. Its width is an upper limit for an energy resolution of 100 meV.[27] In femtosecond time-resolved 2PPE, a first laser pulse h$\nu_1$ photoexcites the sample and, at a variable time delay $\Delta t$, a second laser pulse $h\nu_2$ photoemits the remaining excited electron population, as illustrated by the inset of Fig. 1(b).

The same laser system was used for the transient transmission experiments. As described earlier in detail,[24] 800 nm pulses were used to generate a white light continuum (WLC, 1.77–2.4 eV) by focusing into a sapphire crystal and temporally compressed to 20 fs using a deformable mirror, as described in Ref. 28. In a similar pump–probe scheme to that in 2PPE, h$\nu_1$ photoexcites the sample, and the resulting changes to the transmitted white light are probed after $\Delta t$. 10 nm bandwidth color filters were used to select the desired h$\nu_2$, and the optical signal was detected using a photodiode and a lock-in amplifier. Transient transmission values are normalized to the ground state transmission signal.

## III. RESULTS AND DISCUSSION

### A. Ultrafast dynamics in photoexcited SP6

We begin by examining the non-equilibrium dynamics of photoexcited SP6 on ultrafast time scales using time-resolved 2PPE. Figure 1(a) shows an exemplary measurement of the ultrafast response of a 21 nm SP6 film on ZnO(10-10). The photoinduced change in the 2PPE intensity is plotted in false colors and as a function of electron kinetic energy $E_{kin}$ (vertical axis) and time delay between pump and probe laser pulses (horizontal axis, logarithmic for $\Delta t > 1$ ps). From $\Delta t = 0$ on, a spectrally broad signal is observed

that decays on long picosecond time scales. We extract the time constants of this decay by integrating the 2PPE intensity in eight contiguous 100 meV intervals [see the exemplary pump–probe cross correlation trace in Fig. 1(b), markers]. The data can be reproduced well by fitting triple-exponential decay functions to these traces, convolved with the Gaussian temporal laser pulses' envelope [black curve in Fig. 1(b)]. Figures 1(c)–1(e) depict the energy-dependent relaxation times for the fast (green), intermediate (blue), and slow (purple) time constants.

Before discussing these parameters quantitatively, we compare the time dependence of the 2PPE signal to the time-resolved *optical* response of a similar SP6 film. Such a comparison is not straightforward because the optical spectroscopy is not performed *in situ* under UHV conditions and the two techniques probe the non-equilibrium properties of a sample differently, as illustrated by the energy level diagrams in Fig. 2. While optical spectroscopy is sensitive to energy resonances in a given system, photoelectron spectroscopy provides the absolute binding energies of electronic levels without the need of a resonance condition. However, in molecular systems, the energy of electronic states is highly sensitive to molecular rearrangements and distortions. The resulting inhomogeneous spread of energy levels can have a much stronger impact on absolute energy scales as probed by 2PPE than on the relative level alignment within the individual molecules of a film as measured by optical spectroscopy.[24] In order to still compare the 2PPE and optical data, we integrate the 2PPE intensity across the whole energy range of the spectrally broad signal shown in Fig. 1(a) and compare it (red curve) in Fig. 2 to the change in transmission $\Delta T/T$ for the same probe photon energy $h\nu_{probe}$ = 1.94 eV (markers). Note that $\Delta T/T < 0$ due to excited state absorption and has been multiplied by −1. The two datasets are, up to ~20 ps, in nearly perfect agreement. For larger pump–probe delays, the 2PPE signal shows a slightly slower decay.

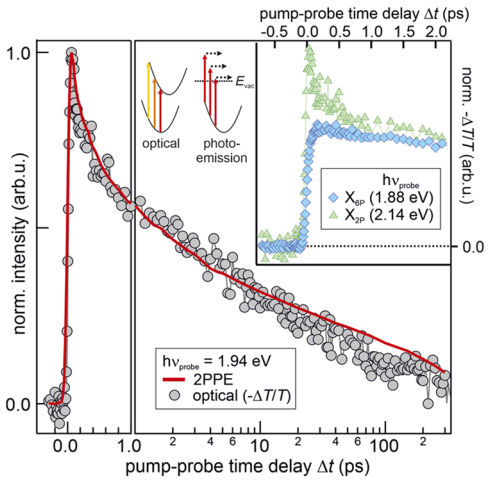


**FIG. 2**. Comparison of time-dependent 2PPE and optical response for the same probe photon energy and similar SP6 films of 21 nm and 20 nm thicknesses, respectively. Optical data were originally published by Elsevier in Ref. 24. $h\nu_{pump}$ = 3.86 eV and 3.70 eV were used in the 2PPE and the optical experiments, respectively. The techniques monitor the excited state's properties differently, on relative and absolute energy scales, as illustrated by the diagram. Inset: only the optical response of the $X_{2P}$ resonance exhibits dynamics on sub-picosecond time scales.

The coincidence of the non-equilibrium response of the two complementary techniques allows for the following assignment of the different time constants extracted from the 2PPE data in Figs. 1(c)–1(e):

(c) The fast time constants vary from 200 to 400 fs as a function of kinetic energy and, as such, as a function of vertical binding energy $E_B = h\nu_{probe} - E_{kin}$ (top red axis), reflecting that electrons with smaller binding energies have a larger phase space for scattering events and, thus, a shorter lifetime. Due to the low excitation densities in our experiment, we exclude electron–electron scattering as a decay mechanism and assign this time constant to fast relaxation due to coupling to the many high-energy vibrational modes of SP6,[26] as, for instance, the CC-stretch modes mentioned in the Introduction. The inset of Fig. 2 compares the transient *optical* signal of the two excited state resonances $X_{6P}$ (diamonds) and $X_{2P}$ (triangles). Clearly, the fast dynamics occur in the $X_{2P}$ resonance only. We conclude that the fast relaxation occurs in $X_{2P}$, which seems to be strongly coupled to high-energy vibrations that allow for fast relaxation.

(d) As for the fast time constants, also the intermediate ones show an energy dependence ranging from 3 ps to 4 ps for increasing vertical binding energies [Fig. 1(d), top axis]. These lie well within the range of internal vibrational relaxation in $X_{6P}$ and $X_{2P}$, $\tau_{IVR}$ = 2 ps–6 ps, as determined in our previous work.[24]

(e) The slow relaxation time is, within error bars, constant for all $E_{kin}$ and $E_B$, respectively. This time constant is with 240(30) ps, in good agreement with the population decay of $X_{2P}$ via intersystem crossing that occurs in SP6 in $\tau_{ISC}$ = 230(50) ps, as determined previously.[24]

Based on these results, we conclude that time-resolved 2PPE of photoexcited SP6 exhibits a nearly one-to-one correspondence to previous optical experiments on a similar sample. The 2PPE response is dominated by the relaxation dynamics in $X_{2P}$, the initial state for ISC. Unfortunately, inhomogeneous broadening on absolute energy scales inhibits spectral characterization of the $X_{6P}$ and the $X_{2P}$ state by 2PPE spectroscopy. This is different in the case of the dark state that occurs as a time-*in*dependent background in all 2PPE spectra, as discussed in Sec. III B. Note that such long-lived signatures can be easily overlooked in femtosecond time-resolved spectroscopic investigations as the time-independent background at negative time delays is routinely subtracted in many pump–probe studies.

## B. Microsecond dynamics of a photostationary state probed by autoionization

Figure 3(a) shows a one-color 2PPE spectrum (blue) measured with $h\nu$ = 3.61 eV and with a repetition rate of $\Delta T_0^{-1}$ = 200 kHz. It is dominated by an intense secondary electron signal which is a cutoff at low energies due to the ionization threshold (work function $\Phi$ = 3.3 eV) of the surface. In addition, the spectrum exhibits a clear, but broad feature (A) centered at 0.6(1) eV well above the secondary electron background. We approximate the

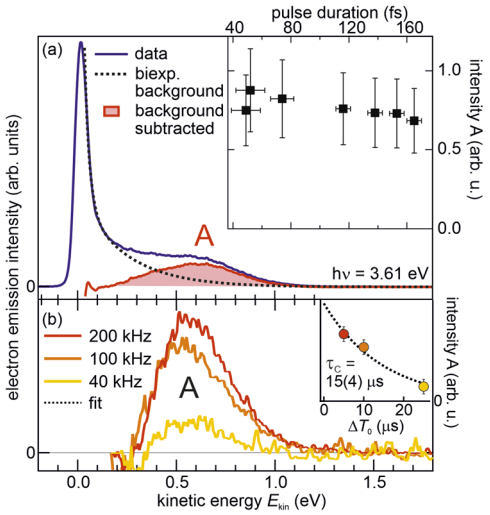


**FIG. 3**. Single-color 2PPE spectra of SP6/ZnO(10-10). (a) Illustration of the secondary electron background (dotted curve) subtraction, h$\nu$ = 3.61 eV; inset: the intensity of peak A is independent of the pulse duration, h$\nu$ = 3.1 eV. (b) Peak A for varying laser repetition rates; inset: intensity of A decreases exponentially with $\Delta T_0$, h$\nu$ = 3.6 eV.

latter with a bi-exponential background (dotted curve) and subtract it from the data. With the photon energy used in this experiment, feature A could originate (i) from an occupied initial state with a vertical binding energy of $E_B = 2 \cdot h\nu_{probe} - E_{kin} = 6.6$ eV, (ii) from a normally unoccupied intermediate state $E_B = h\nu_{probe} - E_{kin} = 3.0$ eV, or (iii) a final state 0.6 eV above the vacuum level. In order to determine the nature of feature A, we first vary the duration of the laser pulses used in the experiment while keeping the photon fluence constant. This stretches the photon density in time.

If feature A were resulting from (i) two-photon photoemission from an initial state, its intensity should depend on the temporal photon density and become smaller upon increasing the laser pulse duration. The same behavior would be expected if A would be a result of (ii) the transient population of an intermediate state with a short lifetime or (iii) a final state as the photoemission signal would be generated by a two-photon process within one laser pulse in these cases, too. The inset of Fig. 3(a) shows the integrated intensity of peak A as a function of laser pulse duration (40–160 fs) at a constant number of photons per pulse. Within the accuracy of this experiment, the intensity of feature A remains constant. The absence of dependence on the laser pulse duration proves that A is not (i) an occupied initial state, not (ii) a short-lived intermediate state A, and not (iii) a final state. In other words, A must be resulting from a long-lived intermediate state with a lifetime likely exceeding the inverse laser repetition rate. These observations are also consistent with the non-trivial fluence dependence of feature A, which will be the subject of Sec. III C.

To test this hypothesis, we vary the repetition rate of the laser system. Figure 3(b) depicts the spectral distribution of A for different laser repetition rates (200 kHz, 100 kHz, and 40 kHz), normalized by the fluence. Clearly, as the repetition rate decreases, the intensity of peak A drops and, in agreement with previous optical experiments,[24] a finite intensity remains for a time delay $\Delta T_0 = 25\ \mu s = (40\ \text{kHz})^{-1}$. The inset of Fig. 3(b) shows the intensity evolution of A as a function of inverse laser repetition rate $\Delta T_0$. The data can be fitted well by a single-exponential decay function (dotted curve), yielding a characteristic time of $\tau_C = 15(4)\ \mu s$. We conclude that peak A results from a normally unoccupied, transiently populated state with a lifetime exceeding the inverse laser repetition rate and likely coinciding with the DS probed in optical spectroscopy previously.[24] Therefore, upon photoexcitation, the SP6 film is in a *photostationary* state, in which population and depopulation of A are balanced. Note that $\tau_C$ does not necessarily reflect the lifetime of the excited state as the variation of the repetition rate may alter the photostationary state non-trivially such that its intensity as a function of $\Delta T_0$ does not have to be dominated by the excited state lifetime.

When probed in photoemission, the spectral position of intermediate electronic states, i.e., the kinetic energy of the photoelectrons, depends on the photon energy h$\nu_{probe}$ used to ionize the sample, as illustrated by the diagram in Fig. 4(a). In single-color 2PPE, h$\nu_{probe}$ is equal to h$\nu_{pump}$, and a variation of the photon energy by $\Delta h\nu$ causes a shift in the spectral signature by the same amount. Figure 4(a) shows the normalized spectral distribution of feature A for different photon energies (right axis), ranging from 1.9 eV to 6.2 eV. Accordingly, if probed in a photoemission process, the spectral signature of the transiently populated, intermediate state A, measured using h$\nu_{probe}$ = 1.9 eV (light green), should shift by $\Delta h\nu = 4.3$ eV, as indicated by the orange arrows. Clearly, this is not the case. Instead, peak A remains at $E_{kin} = 0.7(1)$ eV, corresponding to $E - E_F = 4.0(1)$ eV, where the slightly scattered position of the peak maximum likely results from uncertainties in the background subtraction. This observation demonstrates that A is *not probed in a photoemission process*, where electrons are emitted as a consequence of photon absorption. Instead, the energy information of the laser pulse is "filtered" within the molecular system, making the emitted electrons expose the same $E_{kin}$ irrespective of the photon energy used. This "filtering" must occur via an energy transfer process such as Förster or Dexter transfer, which is initiated by the photoexcitation and eventually leads to autoionization of SP6 molecules by the interaction of two excited states. We note that the absolute intensity of peak A strongly depends on the photon energy and exhibits, in agreement with previous PLE experiments,[23] a maximum at 3.6 eV (not shown).

The spectral shape of feature A can be fitted using the sum of three Gaussian peaks as exemplified for h$\nu_{probe}$ = 1.9 eV in Fig. 4(a). Likely, this progression is a result of a strong coupling of the involved electronic transitions to molecular vibrations in the SP6 molecule. Figure 4(b) shows the energy difference of the two low-energy peaks, $A_1$ and $A_2$, as a function of photon energy, which is constant at 360(40) meV. As shown previously,[24] the ground state vibrational progression of SP6 probed by photoluminescence spectroscopy is characterized by energy quanta of $\hbar\omega = 170(10)$ and 180(10) meV, which can be associated with CC-stretch and C–H-bend modes of the two central fluorenes in SP6 that are connected by the spiro-link (cf. Fig. 1).[26] We conclude that, apparently, two vibrational modes $\hbar\omega$ must be involved in the autoionization process, likely distributed between two excited molecules. Remarkably, the high-energy peak $A_3$ only appears for photoexcitation using photons in the visible range, i.e., smaller photon energies

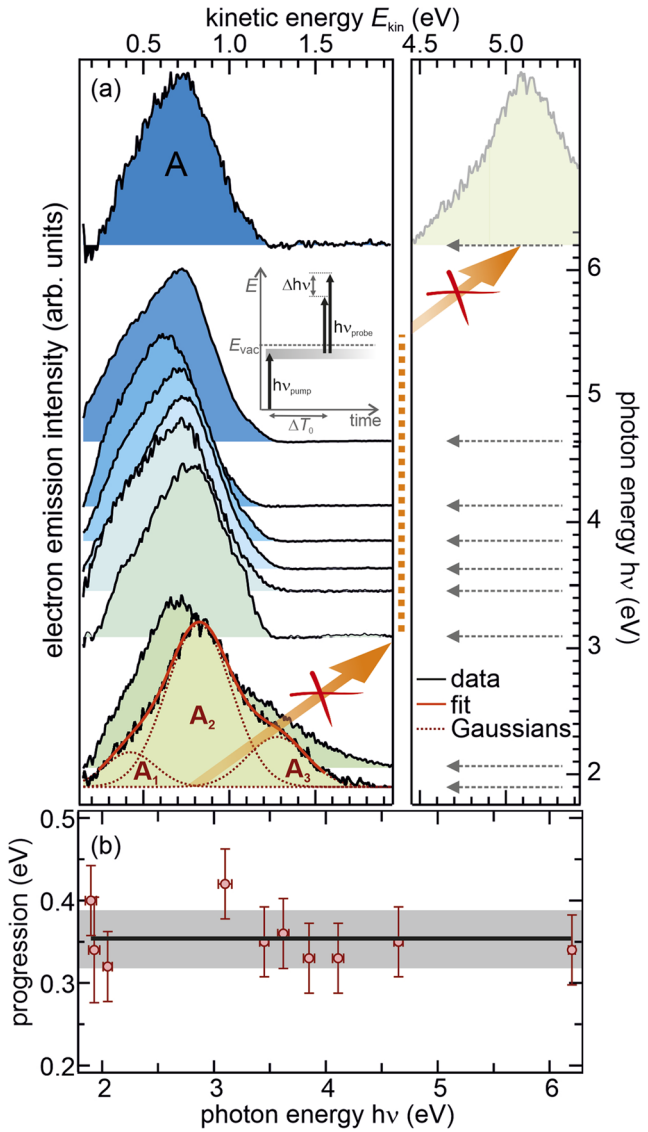


**FIG. 4**. (a) Spectral position of the feature A for varying photon energies (1.9–6.2 eV). The expected spectral shift for a photoemission process (see illustration in the inset) is highlighted by the orange arrows. Spectra are normalized and shifted vertically for clarity and according to the photon energy used in the respective experiment (right axis). Feature A can be fit with the sum of three Gaussian peaks (red curves) separated by 360 meV, as shown in panel (b).

than the absorption gap of SP6.[23] In these experiments, the photoexcitation of SP6 requires the absorption of two photons and a significant electron emission signal, thus, $10^3$ times higher photon fluxes.[29] At these high excitation densities, excited state absorption of A also occurs (in a linear absorption process), thereby depositing a large amount of energy (heat) in the molecular film, which is reflected in the higher vibrational progression at these photon energies.

It should be noted that the comparably clear spectral resolution of the vibrational progression in feature A itself indicates that the electron emission is *not* a photoemission process, but results from intermolecular energy transfer. As discussed in Sec. III A, the amorphous structure of the SP6 film leads to an inhomogeneous broadening of the energy levels, which is reflected significantly more strongly in the photoelectron spectra that probe absolute energies than in the optical data which are sensitive to optical resonances. Similar to the latter, an intermolecular energy transfer is governed by energy differences, allowing us to resolve the vibrational progression in the electron emission signal.

Autoionization by either a Förster or a Dexter energy transfer mechanism requires two interacting excited states. SP6 offers three potential candidates: $X_{6P}$, $X_{2P}$, exhibiting population dynamics on femto- and picosecond time scales, and the long-lived dark state with a lifetime exceeding $\mu$s. In order to identify the excited states involved in the autoionization process, we performed autocorrelation experiments, where the time delay $\Delta t$ between two laser pulses of the same photon energy $h\nu = 3.85$ eV was varied from femtoseconds to nanoseconds. The inset of Fig. 5 displays three exemplary spectra of the feature A: at $t = 0(20)$ fs when pump and probe pulses overlap, at $\Delta t = 150$ ps, and at $\Delta t = 2$ ns. Clearly, the intensity of peak A is unaltered over this large range of time scales. As the ultrafast photoemission and optical experiments clearly showed (cf. Sec. III A and Ref. 24) that both $X_{6P}$ and $X_{2P}$ exhibit dramatic population changes on femto- and picosecond time scales, the sustained intensity of peak A up to 2 ns excludes any involvement of these states in the autoionization process. Thus, peak A can only be originating from long-lived species such as triplets (T), polarons (P), or charge-transfer excitons (CTX). While, in our experiments, we cannot unambiguously exclude CTX–CTX or even mixed interactions (CTX-T, T-P, and CTX-P), autoionization of SP6 by T–T annihilation seems the most simple and likely process, a hypothesis which will be supported further below. Thus, for simplicity, we assume in the following analysis that the dark state is the SP6 triplet state.

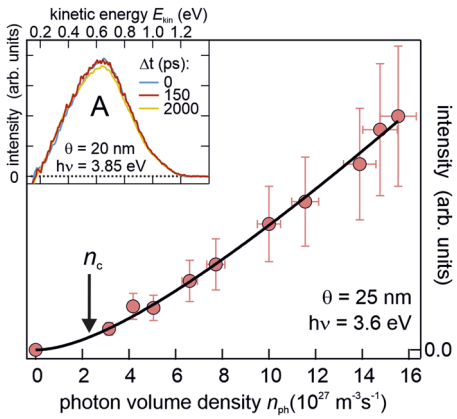


**FIG. 5**. $n_{ph}$ dependence of the electrons emitted by autoionization for a repetition rate of 200 kHz and a laser spot size of $5.5 \cdot 10^{-8}$ $m^2$ (red markers) and the best fit to the data (black curve); see the text for details. Inset: autocorrelation experiment demonstrating the absence of dynamics on ultrafast time scales.

### C. TTA mediated by Dexter transfer

The concentration of excited states does not change in a photostationary state. Approximating the pulsed excitation at 200 kHz > $(T_0)^{-1}$ as a continuous wave, the time-dependent change in the triplet concentration $n_T$ must vanish, as described in the literature previously,[30]

$$\frac{dn_T}{dt} = \alpha n_{ph} - k_D n_T - k_{TTA} n_T^2 = 0. \quad (4)$$

In this case, all decay channels of $n_T$ are balanced by the continuous repopulation. Here, $\alpha$ is the population probability, $n_{ph}$ the photon volume density, $k_D$ the intrinsic triplet decay rate (excluding decay by TTA), and $k_{TTA}$ the rate constant of TTA (in units of $m^3\ s^{-1}$). With the characteristic photon volume density,[31]

$$n_c = \frac{k_D^2}{k_{TTA}}, \quad (5)$$

that defines the crossover between intrinsic triplet decay and TTA-dominated decay dynamics,[30] the solution of Eq. (4) becomes

$$n_T(n_{ph}) = \frac{1}{2}\frac{n_c}{k_D}\left(\sqrt{1 + 4\alpha\frac{n_{ph}}{n_c}} - 1\right). \quad (6)$$

The photon volume density dependence of the electron emission signal,

$$I_{EE}(n_{ph}) = p \cdot k_{TTA} \cdot n_T^2(n_{ph}) \cdot V = pV\left(\frac{1}{2}n_c + \alpha n_{ph} - \sqrt{\left(\frac{1}{2}n_c\right)^2 + \alpha n_{ph} \cdot n_c}\right), \quad (7)$$

depends quadratically on the triplet density $n_T(n_{ph})$ in the experiment. The prefactor $p$ accounts for the finite detection probability of emitted electrons, and the population probability,

$$\alpha = \frac{A_{2P}}{A_{2P} + A_{6P}} = 0.27, \quad (8)$$

can be approximated[32] by the intensity ratio of the $X_{2P}$ and $X_{6P}$ optical resonances from Ref. 24.

Figure 5 shows the dependence of the electron emission intensity on the absorbed photon volume density. If feature A were resulting from an ordinary one- or two-photon process within one laser pulse, its intensity should scale linearly or quadratically, respectively. This is not the case. When fitted with a power law (not shown), the electron emission intensity dependence on $n_{ph}$ exposes an exponent of 1.5. This confirms the conclusion of Sec. III B that the detected spectral signature is not composed of *photo*electrons, but that electron emission occurs as a consequence of excited state interaction. Using Eq. (7), where $n_{ph}$, $V$, and $\alpha$ are known experimental parameters, the curvature of the $n_{ph}$ dependence of the electron emission signal is solely determined by the characteristic photon volume density $n_c$. Our least squares fit (black) yields $n_c = 2.3(7)\cdot 10^{27}\ m^{-3}\ s^{-1}$ as indicated by the arrow in Fig. 5, showing that for the photon densities applied, TTA is dominating the triplet decay. This is consistent with the major electron emission observed in the experiment.

In order to determine whether the TTA is mediated by Förster or Dexter transfer processes, we first calculate the quantum efficiency per triplet for TTA from our data using

$$\Phi_{TTA} = \frac{k_{TTA} \cdot n_T}{k_D + k_{TTA} \cdot n_T} = \frac{I_{EE}(n_{ph})}{\alpha n_{ph} \cdot pV}, \quad (9)$$

which is a direct consequence of Eqs. (4)–(7), and plot it as a function of photon volume density (bottom axis) in Fig. 6 (red circles). Remarkably, the TTA quantum efficiency lies between 22% and 50% for the excitation densities used in the experiment. For comparison, we also provide the corresponding photon area densities $\rho_{ph}$ on the top axis.

With Eqs. (1)–(3) for Förster and Dexter energy transfers, we can also formulate mathematical expressions for the TTA quantum efficiency in the case of Dexter energy transfer,

$$\Phi_{TTA}^{Dex}(n_{ph}) = \left[1 + \exp\left(-\frac{2r_{Dex}}{L}\left(1 - \frac{d_T(n_{ph})}{r_{Dex}}\right)\right)\right]^{-1}, \quad (10)$$

and in the case of Förster energy transfer,

$$\Phi_{TTA}^{F}(n_{ph}) = \left[1 + \left(\frac{d_T(n_{ph})}{r_F}\right)^6\right]^{-1}, \quad (11)$$

where

$$d_T(n_{ph}) = 2 \cdot \sqrt[3]{\frac{3}{4\pi \cdot n_T(n_{ph})}}. \quad (12)$$

These can be used to fit the experimental $\Phi_{TTA}$ in Fig. 6 (solid and dashed curves, respectively). We approximate the mean van der Waals distance between two SP6 molecules by using

$$L = 2 \cdot \sqrt[3]{\frac{3}{4\pi \cdot \rho}}, \quad (13)$$

with the SP6 density $\rho = 1.14 \cdot 10^{27}\ m^{-3}$. Clearly, the distance dependence of the Förster-type transfer (gray dashed curve) does not

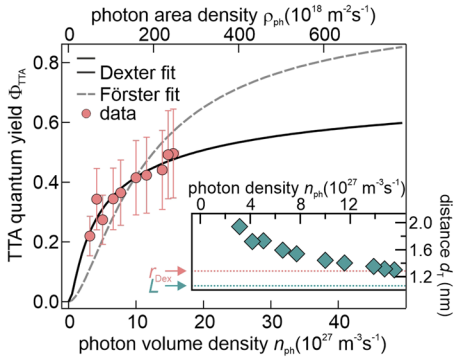


**FIG. 6.** The photon density dependence of the experimental TTA quantum efficiency (red circles) is well-fitted for Dexter-type energy transfer *en route* to autoionization (black curve). Förster-type transfer (dashed curve) cannot account for the slope of the experimental data. Inset: average triplet distance for varying $n_{ph}$.

follow the experimental trend and can, therefore, be excluded. The quantum efficiency for Dexter-mediated TTA [Eq. (10), black solid curve], on the contrary, provides a perfect fit to the data with only two free parameters. It yields a Dexter radius of $r_{Dex}$ = 1.3(2) nm and an intrinsic triplet lifetime of $\tau_D = k_D^{-1}$ = 0.10(3) s. This enables the calculation of the rate constant for TTA based on Eq. (5) to be only $k_{TTA}$ = 4.5 $10^{-26}$ $m^3$ $s^{-1}$. This extraordinarily small value lies eight orders of magnitude below typical literature values[33] and cannot solely be explained by the absence of spin statistics in our model. The, nevertheless, significant TTA quantum efficiency (Fig. 6) can only be resulting from an extraordinarily high triplet density.

With Eqs. (12) and (6), we can calculate the average triplet distance as a function of photon density as displayed in the inset of Fig. 6. For all excitation densities used in our experiment, the triplet–triplet distance is very small with less than 2 nm. With increasing fluence, it even decreases and approximates the Dexter radius $r_{Dex}$ (red) and the van der Waals distance of two SP6 molecules $L$. These small distances, i.e., high triplet densities explain the 50% large TTA quantum efficiency despite the extremely low TTA rate constant $k_{TTA}$.

Based on the above, it is possible to calculate the external quantum efficiency (EQE) for photoinduced electron emission through autoionization,

$$\Phi_{AI} = \alpha \cdot \Phi_{TTA}, \tag{14}$$

which is plotted (circles) in Fig. 7 as a function of incident photon area density (top axis) and irradiance (bottom axis). We calculate the expected excitation density-dependent evolution of the EQE for the autoionization process based on the above model using Eqs. (10) and (14). This is displayed by the dotted curve in Fig. 7 and extrapolates to a maximum of 25% for highest photon fluxes. Figure 7 also shows the experimental (diamonds) and extrapolated current densities $j = \Phi_{AI} \cdot \rho_{ph} \cdot e$ (right axis), where $e$ is the elementary charge. The highest current density in our experiments amounts to 0.5 mA $cm^{-2}$. In the range of solar irradiance on the order of 100 W $m^{-2}$ eV at similar photon energies,[34] the extrapolated EQE for electron emission and the corresponding current density $j$ are on the order of 15% and 1.5 mA $cm^{-2}$, respectively.

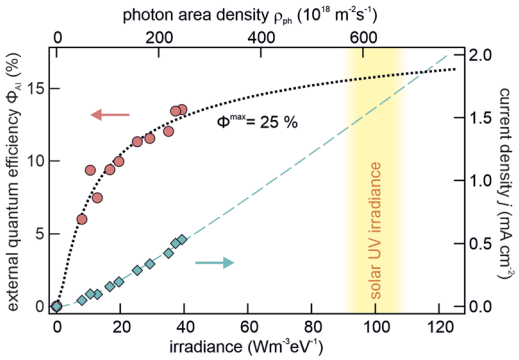


**FIG. 7.** EQE (left axis) and current density (right axis) for the illumination of condensed SP6 as measured (markers) using h$\nu$ = 3.6 eV and calculated based on the TTA model with Dexter-type energy transfer (dotted and dashed curves).

In summary, the TTA model describes the excitation density-dependent evolution of our data very well, allowing for the calculation of the TTA quantum efficiency as a function of photon density, which behaves as expected for Dexter-type energy transfer of the triplets. The very high probability for a triplet to undergo TTA (49% at the largest triplet density in our experiments) can be translated to a sizable EQE of $\Phi_{AI} = \alpha \cdot \Phi_{TTA}$ = 13% at highest experimental excitation densities, which corresponds to a current density $j$ = 0.5 mA $cm^{-2}$.

It should be noted that the above model is not restricted to Dexter-type TTA, but could be directly translated to CTX–CTX annihilation. For electron emission due to mixed interactions, such as CTX-P (cf. Sec. III B), the mathematical framework would stay similar, albeit with a larger number of free parameters. The extracted high triplet density in our experiments, very close to the SP6 density, displayed in the inset of Fig. 6, however, is a strong indication that the underlying mechanism is, indeed, TTA, as such a dense distribution of CTX with or without polarons is physically not possible.

## D. Discussion and conclusions

Figure 8(a) summarizes the pathways of optical excitations in SP6 layers, and Table I displays all relevant experimental parameters determined in this work. As shown previously,[24] photoexcitation of SP6 leads to the population of two separate electronic states, $X_{6P}$ and $X_{2P}$. Excess energy is released by internal vibrational relaxation on femto- and picosecond time scales, which is equivalently monitored by time-resolved photoelectron and optical spectroscopies (cf. Sec. III A). $X_{6P}$, which is localized on the 6P unit of the molecule, decays by fluorescence and diffusion-limited electron transfer to the ZnO substrate. $X_{2P}$ solely decays into a dark state with a time constant of $\tau_{ISC}$ = 240(30) ps that is consistently measured by photoelectron and optical spectroscopies. This dark state, likely the SP6 triplet, exhibits a long lifetime, which enables Dexter-type energy transfer of the triplet excitation. Beyond relaxation, it decays by TTA, leading to autoionization of SP6 molecules. The resulting electron emission appears as a photon energy-independent peak in the photoelectron spectra. A comparable signature was first observed in 2PPE of Ag(111) in 1985[35] and described as a result of plasmon–plasmon annihilation by Petek and co-workers only recently.[36] Electron emission through two particle annihilation, thus, seems to be a general mechanism that occurs in very different materials and on varying time scales. In the present case, it exhibits a vibrational progression with energy quanta of twice the CC-stretch and CH-bend modes dominating the vibrational ground state progression.[26] Using the literature value for the highest occupied molecular orbital (HOMO) of SP6 of $E - E_F$ = −1.7 eV,[23] we estimate the triplet resonance energy to 2.8 eV. This corresponds to a triplet level at $E - E_F$ = 1.1 eV above the Fermi energy, which is equal to a vertical binding energy of $E_B$ = 2.2 eV.

Based on excitation density-dependent experiments and a simple rate equation model, we demonstrate that Dexter energy transfer is the rate-limiting step in the TTA process. As illustrated in Fig. 8(b), this can proceed via direct Dexter transfer from one of the involved triplets (A) to the other (B), resulting in one molecule in the ground state and the other in a doubly excited singlet state.

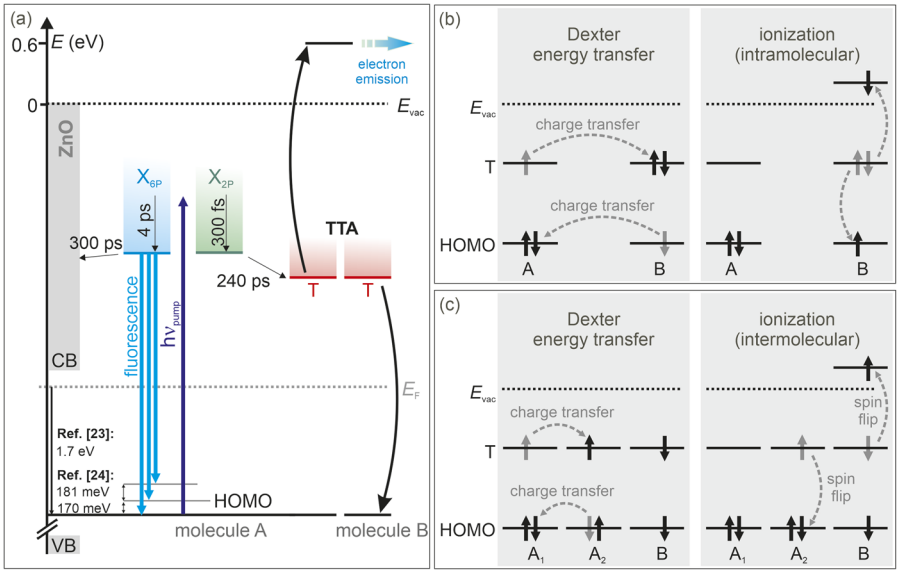


**FIG. 8**. (a) Overview of the elementary processes occuring in the SP6 film upon UV photoexcitation. (b) Dexter-type TTA followed by intramolecular Auger decay where a doubly excited state couples to a continuum.[37] (c) Dexter triplet energy transfer followed by intermolecular Auger decay leading to TTA. See the text for details.

The latter relaxes by intramolecular Auger decay going along with electron emission. In the alternative relaxation pathway, depicted in Fig. 8(c), the triplet excitation of molecule $A_1$ is (Dexter) transferred to a molecule $A_2$, which was originally in its ground state and is in the closest vicinity of the second triplet residing on molecule B. The TTA then occurs in a second step by *inter*molecular Auger decay that requires a spin flip in order to transform the triplets into singlets. Although, based on our data, we cannot unambiguously exclude either scenario, the second one, which involves (i) a Dexter energy transfer process to a nearest neighbor of a second triplet, (ii) strongly distance-dependent intermolecular Auger decay, and (iii) a spin flip process, seems highly improbable. Based on this, we conclude that direct Dexter-type TTA followed by intramolecular Auger decay (without spin flip) is most likely the accurate description of the processes investigated in this work.

Based on the rate equation model, we also determine the characteristic photon density for TTA, intrinsic triplet lifetime, TTA rate constant, Dexter radius, as well as the EQE and current density in the experiment as listed in Table I. The latter two are, with 15% and 1.5 mA cm$^{-2}$ at solar UV irradiances, respectively, quite high for an illuminated, pure, and mono-molecular organic film, which is not a complex heterostructure as in current organic light-harvesting devices. The chemical potential between the electron and the hole after successful TTA is larger than 4.0 eV and, thus, very high. The power conversion efficiency is defined as

$$\mathrm{PCE} = \mathrm{FF} \cdot \frac{P_{\mathrm{out}}}{\mathrm{h}\nu \cdot \rho_{\mathrm{ph}}^{\mathrm{solar}}}, \tag{15}$$

where FF is the unknown fill factor and $P_{\mathrm{out}}$ is the output power achieved under illumination. In order to use SP6 in tandem solar cells as the UV-active material, it would need to have a PCE in the UV range that is compatible with the overall PCE of current organic solar cells of up to 17%, which is determined across the whole solar spectrum. With $P_{\mathrm{out}} = 4\ \mathrm{V} \cdot j_{\mathrm{solar}}$, solar photon density $\rho_{\mathrm{ph}}^{\mathrm{solar}} = 600 \cdot 10^{18}\ \mathrm{m}^{-2}\,\mathrm{s}^{-1}$ at $\mathrm{h}\nu = 3.6$ eV, the wavelength-specific PCE of SP6 amounts to PCE = FF · 17%. With typical fill factors clearly above 0.5, SP6 may be a promising material for forthcoming organic tandem cells. Moreover, this work is the proof of principle of highly efficient electron emission through TTA. We hope that our work stimulates the design of new organic molecules that exhibit or even exceed the fundamentally necessary properties of SP6 that enable efficient autoionization: matching binding energies $E_{\mathrm{B}}^{\mathrm{T}} < \frac{1}{2} \cdot E_{\mathrm{B}}^{\mathrm{S_0}}$ of triplet and ground states with respect to the ionization potential, respectively, characteristic photon densities $n_{\mathrm{c}}$ in the $10^{27}\ \mathrm{m}^{-3}\,\mathrm{s}^{-1}$ range, and a large packing density of the molecules. Organic materials with these properties and possibly even absorption in the *visible* light range seem highly promising for future light-harvesting applications.

**TABLE I**. Summary of parameters extracted using the TTA model.

| | | |
|---|---|---|
| IVR time (fast) | $\tau_{\mathrm{IVR1}}$ | 200–400 fs |
| IVR time (slow) | $\tau_{\mathrm{IVR2}}$ | 2–6 ps |
| ISC time | $\tau_{\mathrm{ISC}}$ | 240(30) ps |
| Triplet lifetime | $\tau_{\mathrm{D}}$ | 0.10(3) s |
| TTA rate constant | $k_{\mathrm{TTA}}$ | $4.5 \cdot 10^{-26}\mathrm{m}^3\ \mathrm{s}^{-1}$ |
| Dexter radius | $r_{\mathrm{Dex}}$ | 1.3(2) nm |
| EQE. . . | | |
| . . .at solar UV irradiances | $\Phi_{\mathrm{AI}}^{\mathrm{solar}}$ | 15% |
| . . .maximum | $\Phi_{\mathrm{AI}}^{\mathrm{max}}$ | 25% |
| Current density | | |
| . . .at solar UV irradiances | $j_{\mathrm{solar}}$ | 1.5 mA cm$^{-2}$ |

## ACKNOWLEDGMENTS

This work was funded by the Deutsche Forschungsgemeinschaft (DFG, German Research Foundation) Project-ID No.

182087777-SFB 951. Additional funding was granted by the European Union through Grant No. 280879-2 CRONOS CP-FP7. The authors thank Emil List-Kratochvil for fruitful discussions, Sylke Blumstengel for providing the SP6 molecules, and Mino Sparenberg for their density determination, as well as Selene Mor for technical support during autocorrelation experiments. S.V. would like to thank the Max Planck Research Society for a Max Planck Postdoctoral Fellowship.

## REFERENCES

[1]S. Blumstengel, S. Sadofev, and F. Henneberger, "Electronic coupling of optical excitations in organic/inorganic semiconductor hybrid structures," New J. Phys. **10**, 065010 (2008).
[2]Y. Y. Cheng, A. Nattestad, T. F. Schulze, R. W. MacQueen, B. Fuckel, K. Lips, G. G. Wallace, T. Khoury, M. J. Crossley, and T. W. Schmidt, "Increased upconversion performance for thin film solar cells: A trimolecular composition," Chem. Sci. **7**, 559 (2016).
[3]J. C. Goldschmidt and S. Fischer, "Upconversion for photovoltaics – a review of materials, devices and concepts for performance enhancement," Adv. Opt. Mater. **3**, 510 (2015).
[4]K. Borjesson, D. Dzebo, B. Albinsson, and K. Moth-Poulsen, "Photon upconversion facilitated molecular solar energy storage," J. Mater. Chem. A **1**, 8521 (2013).
[5]L. Wondraczek, E. Tyystjärvi, J. Méndez-Ramos, F. A. Müller, and Q. Zhang, "Shifting the sun: Solar spectral conversion and extrinsic sensitization in natural and artificial photosynthesis," Adv. Sci. **2**, 1500218 (2015).
[6]R. Schlesinger, F. Bianchi, S. Blumstengel, C. Christodoulou, R. Ovsyannikov, B. Kobin, K. Moudgil, S. Barlow, S. Hecht, S. Marder, F. Henneberger, and N. Koch, "Efficient light emission from inorganic and organic semiconductor hybrid structures by energy-level tuning," Nat. Commun. **6**, 6754 (2015).
[7]R. Friedlein, "Two-photon photoionization by singlet-singlet annihilation in polycrystalline, thin perylene films," Appl. Phys. A **95**, 315 (2009).
[8]C. A. Parker and C. G. Hatchard, "Delayed fluorescence from solutions of anthracene and phenanthrene," Proc. R. Soc. London, Ser. A **269**, 574 (1962).
[9]M. Pope and J. Burgos, "Charge-transfer exciton state and ionic energy levels in anthracene crystal," Mol. Cryst. **1**, 395 (1966).
[10]D. Haarer and G. Castro, "Exciton induced photoemission in anthracene," Chem. Phys. Lett. **12**, 277 (1971).
[11]W. Shockley and H. J. Queisser, "Detailed balance limit of efficiency of *p-n* junction solar cells," J. Appl. Phys. **32**, 510 (1961).
[12]J. R. Tritsch, W.-L. Chan, X. Wu, N. R. Monahan, and X.-Y. Zhu, "Harvesting singlet fission for solar energy conversion via triplet energy transfer," Nat. Commun. **4**, 2679 (2013).
[13]C. A. Parker, "Sensitized *p*-type delayed fluorescence," Proc. R. Soc. London, Ser. A **276**, 125 (1963).
[14]T. N. Singh-Rachford and F. N. Castellano, "Low power visible-to-UV upconversion," J. Phys. Chem. A **113**, 5912 (2009).
[15]V. Gray, D. Dzebo, M. Abrahamsson, B. Albinsson, and K. Moth-Poulsen, "Triplet–triplet annihilation photon-upconversion: Towards solar energy applications," Phys. Chem. Chem. Phys. **16**, 10345 (2014).
[16]S. Arnold, M. Pope, and T. K. T. Hseih, "Double quantum external photoelectric effect in crystalline tetracene," Phys. Status Solidi B **94**, 263 (1979).
[17]J. Wessel, "Biexcitonic autoionization in naphthalene trimer clusters," Phys. Rev. Lett. **64**, 2046 (1990).
[18]M. Ono and M. Kotani, "Time-resolved measurement of excitonic electron emission from a fluoranthene crystal," Chem. Phys. Lett. **295**, 493 (1998).
[19]We use the term autoionization in its broadest sense, "self-ionization" of a molecule regardless of the underlying energy transfer process, i.e., broader than the original definition introduced by Fano[37] that requires a doubly excited state coupled to a continuum.
[20]M. R. Narayan and J. Singh, "Excitonic processes in organic semiconductors and their applications in organic photovoltaic and light emitting devices," in *Excitonic and Photonic Processes in Materials*, Springer Series in Materials Science Vol. 203 (Springer, 2015), p. 229.
[21]D. Lapiano-Smith, K. Lee, C. I. Ma, K. Wu, and D. M. Hanson, "Auger decay and autoionization of core hole excited states in molecular oxygen," J. Electron Spectrosc. Relat. Phenom. **51**, 221 (1990).
[22]A. Roos, J. Eland, J. Andersson, R. Squibb, D. Koulentianos, O. Talaee, and R. Feifel, "Abundance of molecular triple ionization by double auger decay," Sci. Rep. **8**, 16405 (2018).
[23]S. Blumstengel, S. Sadofev, C. Xu, J. Puls, R. Johnson, H. Glowatzki, N. Koch, and F. Henneberger, "Electronic coupling in organic-inorganic semiconductor hybrid structures with type-II energy level alignment," Phys. Rev. B **77**, 085323 (2008).
[24]L. Foglia, L. Bogner, M. Wolf, and J. Stähler, "Localization-dependent charge separation efficiency at an organic/inorganic hybrid interface," Chem. Phys. Lett. **646**, 25 (2016).
[25]The SP6 density was determined by Mino Sparenberg (Humboldt University Berlin).
[26]J. Stähler, O. T. Hofmann, P. Rinke, S. Blumstengel, F. Henneberger, Y. Li, and T. F. Heinz, "Raman study of 2,7-bis(biphenyl-4-yl-)2',7'-ditertbutyl-9,9'-spirobifluorene adsorbed on oxide surfaces," Chem. Phys. Lett. **584**, 74 (2013).
[27]J. Stähler and P. Rinke, "Global and local aspects of the surface potential landscape for energy level alignment at organic-zno interfaces," Chem. Phys. **485**, 149 (2017).
[28]D. Wegkamp, D. Brida, S. Bonora, G. Cerullo, J. Stähler, M. Wolf, and S. Wall, "Phase retrieval and compression of low-power white-light pulses," Appl. Phys. Lett. **99**, 101101 (2011).
[29]Note that, at these low photon energies, the excitation of A requires two photons within one laser pulse and, thus, a strong dependence on the pulse duration is expected. The absence of such dependence for hν = 3.1 eV in Fig. 3 conversely shows that, despite being significantly below the absorption maximum of SP6, excitation still occurs in a one-photon process.
[30]O. V. Mikhnenko, P. W. M. Blom, and T.-Q. Nguyen, "Exciton diffusion in organic semiconductors," Energy Environ. Sci. **8**, 1867 (2015).
[31]The volume V is calculated using the laser spot size $A = 5.5 \cdot 10^{-8}$ m$^2$, the optical penetration depth $\lambda = 25$ nm[23] in SP6, and the SP6 layer thickness of 25 nm.
[32]This approximation assumes, following the line of arguments in Ref. 24, that all molecules excited to $X_{2P}$ undergo ISC to the triplet state.
[33]A. Ligthart, X. de Vries, L. Zhang, M. C. W. M. Pols, P. A. Bobbert, H. van Eersel, and R. Coehoorn, "Effect of triplet confinement on triplet–triplet annihilation in organic phosphorescent host–guest systems," Adv. Funct. Mater. **28**, 1804618 (2018).
[34]C. A. Gueymard, "The sun's total and spectral irradiance for solar energy applications and solar radiation models," Solar Energy **76**, 423–453 (2004).
[35]K. Giesen, F. Hage, F. Himpsel, H. J. Riess, and W. Steinmann, "Two-photon photoemission via image-potential states," Phys. Rev. Lett. **55**, 300 (1985).
[36]M. Reutzel, A. Li, B. Gumhalter, and H. Petek, "Nonlinear plasmonic photoelectron response of Ag(111)," Phys. Rev. Lett. **123**, 017404 (2019).
[37]U. Fano, "Effects of configuration interaction on intensities and phase shifts," Phys. Rev. **124**, 1866 (1961).